Imaging ion outflow in the high-latitude magnetosphere using low-energy neutral atoms

M. Hesse, M. F. Smith, and F. Herrero

Code 696, NASA/Goddard Space Flight Center, Greenbelt, MD

A. G. Ghielmetti, and E. G. Shelley

Lockheed Palo Alto Research Laboratory, Palo Alto, CA

P. Wurz, and P. Bochsler

University of Bern, 3012 Bern, Switzerland

D. L. Gallagher, and T. E. Moore

NASA/Marshall Space Flight Center, Huntsville, AL

T. Stephen

University of Denver, Denver, CO

ABSTRACT

The measurement of neutral atom fluxes generated by charge exchange with the Earth's geocorona has recently been shown to provide the capability to image the magnetosphere. Here we investigate neutral oxygen fluxes, produced by charge exchange from the cusp/cleft ion fountain population. Using an empirical cusp/cleft ion fountain model, an empirical variation of the geocoronal neutral hydrogen density with distance, and typical values for charge exchange cross-sections, line-of-sight integrations are performed to calculate the neutral oxygen flux at arbitrary locations in space. The resulting images are evaluated for a set of orbital positions of the proposed HI-LITE small explorer spacecraft. It is shown that the resulting neutral oxygen fluxes are high enough for imaging with a low energy neutral atom imaging instrument (ILENA) on board the spacecraft.

1. INTRODUCTION

A major objective of space physics is to understand the Earth's magnetosphere and its interaction with the ionosphere and solar wind. Nowhere is that interaction more readily apparent, or more highly variable, than in the high- latitude regions of the Earth's magnetosphere. Input from the solar wind produces significant effects on the Earth's ionosphere including auroral displays and upwelling of ionospheric ions that ultimately become part of the magnetospheric population, and interact back on the ionospheric plasma. When the amount of solar wind mass, energy, and momentum added to the magnetosphere is high, the system becomes highly disturbed and the energy imparted to the system is dissipated explosively through the substorm process. The high-latitude magnetosphere plays a central role in this dynamic, energy dissipation process. In the interaction of the solar wind with the ionosphere, the Earth's ionosphere at high latitudes has two principal roles. First, it allows closure of magnetospheric current systems and acts in conjunction with the neutral atmosphere as a damper of plasma motions driven by the solar wind (i.e., ion drag). Second, it acts as an important source of plasma for the magnetosphere, owing in part to the energy dissipation associated with the damping of solar-wind driven plasma motions. We know from statistical sampling of a large number of in situ measurements that ion outflow from the high-latitude regions is substantial[1]. Depending on the level of solar and magnetospheric activity, ionospheric ions can contribute from a small fraction to nearly all of the plasma in the Earth's plasma sheet[2,3]. The dynamics of the ion outflow from particular regions within the high-latitude ionosphere are different. The outflow from the polar cap, called the polar wind, is continuously present. It consists of light ions (few eV H^+ and He^+) and is relatively independent of interplanetary conditions and geomagnetic activity[4]. The outflow from the high latitude auroral regions is much more dynamic, contains heavy ions such as O^+, and is correlated with both geomagnetic and solar activity[1,5].

0-8194-1257-0/93/$6.00

Studies have indicated that the auroral acceleration region is an important, if not dominant, region of ion outflow[6,7]. However, the discovery of the cleft ion fountain[8,9,10,11] and subsequent interpretation of the ion outflow in this region[8] indicate that it is also an important source of low energy ions in the polar cap, and ultimately, in the plasma sheet. Since thermal O^+ in the ionosphere is gravitationally bound, its escape from the high-latitude regions requires a pre-energization mechanism[12]. The other major outflowing species, H^+, is not gravitationally bound and acquires its energy above ~1000 km, where thermal H^+ dominates the cold plasma. Both ion species are limited by charge exchange with the geocorona neutral H[13,14]. This charge exchange process give rise to an intense flux of neutral O and H in the high-latitude magnetosphere[15].

More than 20 years after the discovery of O^+ in the high-latitude region and the realization that the ionosphere is a significant contributor of magnetospheric plasma[16], the primary region of low energy ion outflow remains controversial. Furthermore, the possibilities are diametrically opposite: On the one hand it is supposed that an intense localized cusp is providing the ionospheric ions for the magnetosphere, and on the other hand the source is speculated to be a diffuse extensive region comprising the entire auroral zone. One possibility is that both interpretations of the data are correct. For example, one region is the dominant outflow source for one level of geomagnetic activity, while the other source dominates for other conditions. However, it is important to realize that the failure to resolve this controversy is due precisely to the limitations of in situ measurements. The global perspective is produced only by interpretation of a large number of individual, localized measurements which do not resolve temporal or spatial relationships between various regions. Resolution of these issues requires global imaging of the high-latitude ion outflow regions on time scales commensurate with the solar wind-magnetosphere interaction cycle since individual source region may be dominant for specific phases of a substorm or for different levels of solar and/or magnetospheric activity.

One of the fundamental dynamical features of the Earth's magnetosphere is the substorm. Some of the energy released during a substorm is transferred to the inner magnetosphere where it appears as ring current enhancement, Joule heating in the ionosphere, and auroral particle precipitation, while the rest of the energy is returned to the solar wind through the geomagnetic tail. Eventually, the magnetosphere recovers from the explosive dissipation phase and energy begins to be stored again in the magnetotail until the next substorm is triggered. The entire process of explosive dissipation and recovery takes an average of about one to two hours and recurs every few hours if energy transfer from the solar wind continues at a high rate (i.e., the IMF remains southward). Much of the phenomenology of the substorm process has a firm observational basis. Baker et al.[17] argued that a reduction of the plasma sheet half- width during the substorm expansion phase should lead to a demagnetization of O^+ ions of ionospheric origin and enhanced growth of a large-scale ion tearing instability believed to initiate the substorm explosive growth. It is also well documented that larger relative oxygen ion densities are observed in the plasma sheet after the expansion phase than during the growth phase[18]. This O^+ must be supplied from the high latitude region during the substorm. In addition, the ionospheric ions in the plasma sheet may cause important differences between strings of multiple substorms and isolated substorms. Considering the potential importance of ionospheric ions in the substorm process, there have been suprisingly few investigations of the ionospheric ion source and its dependence on interplanetary and substorm conditions[19]. Part of the problem in investigating the ion source morphology with in situ measurements is the difficulty in determining the dominant region of ion outflow. However, in the case of substorms the difficulty with the in situ measurements is much greater than a simple spatial issue since different segments of the high latitude region may be important at different phases of the magnetospheric substorm. Hence, in situ measurements provide either a snapshot of ion outflow in a very localized region or a statistical sample of a large region lacking any sort of temporal information. Neither of these can be used to determine the importance of ionospheric ions in the substorm process on a global scale. The resolution of these issues requires global imaging of ion outflow over timescales appropriate to the substorm process (5 minutes over total characteristic times of 1 hour). With these measurements, spatial variations of the ion outflow will be separated from temporal changes related to the substorm process and the importance of the ionospheric ions to the substorm process will be determined. Based on concurrent, simultaneous observations of the HI-LITE instruments and low altitude data, we will determine the relative positioning of ion outflow and magnetospheric boundaries. For example, from the shape of the upwelling plume it can be determined whether the ion outflow occurs on sunward or antisunward convecting field lines and how the outflow is related spatially to substorm features such as westward travelling surges, which are at the base of the evening side of the substorm current wedge[20]. The observations of the spatial distribution could also be combined with magnetic mapping using current models[21] to assess the expected magnetotail plasma injection region.

In this paper we use a cusp ion fountain model, recently developed by Gallagher (paper in preparation), to provide the source ion fluxes for the charge exchange process and subsequent line of sight integrations to estimate the observable fluxes at the spacecraft location. In the following we will demonstrate that neutral atom imaging of the cusp/cleft ion fountain is feasible using the ILENA instrument (Ghielmetti et al., this issue) (proposed as part of the HI-LITE mission (Smith et al., this issue)) and will lead to images of both the spatial and temporal evolution necessary to assess the role of the ion fountain in magnetospheric processes.

2. NEUTRAL ATOM IMAGING

2.1. Charge exchange

Neutral atom imaging is a new technique that enables global imaging of magnetospheric plasmas to be undertaken[22]. Briefly, the Earth's geocorona acts like an imaging screen for ions in the ionosphere/magnetosphere. These ions charge exchange with the Earth's geocorona producing neutral atoms. The neutrals produced in this reaction leave the interaction region with essentially the same energy as the outflowing ion. In addition, the direction of the neutral is that of the ion at the moment of the interaction, i.e., the combination of gyromotion and motion along the field. The neutral then travels in a almost straight line to the imaging point, modified only by gravitational acceleration. For the lowest energies (~10eV), this leads to an appreciable angular distortion, estimated to be $< 14^o$ for 10eV O^+ at a distance of $1R_E$ from the source region, which are, however, an upper limit to the possible distances during the projected HI-LITE orbit (see Smith et al., this issue). For energies of 30eV and above, the angular deflection is less than 4.6^o, below the limit of the angular resolution of $6^o \times 6^o$ for each pixel. Therefore, energy channels above 30 eV will make it possible to produce an image of the input ion energy and direction by collecting and analyzing the neutrals. Despite the distortion, energies below 30 eV can be used for imaging at distances closer to the source, and will provide the total low energy source flux in any case. Both the density of the Earth's geocorona and the cross sections for H^+ and O^+ on H and O neutrals are well known. It is thus possible to calculate a neutral flux leaving an interaction region for any specified O^+ or H^+ distribution.

2.2. Cleft ion fountain

A region of intense O^+ transverse ion energization to energies 10 eV has been identified extending from 2,000 to 10,000 km on the dayside of the magnetosphere. Although the association of the upwelling ions with field- aligned currents suggested that Joule heating was an important energy source, Moore et al.[23] were unable to identify the driving energy source using in situ measurements from one pass through the region. However, recently Whalen et al.[24] have obtained data with higher temporal and energy resolution and concluded from the satellite and earlier rocket observations that the localized upwelling ion region is the high-altitude, dayside component of a Transverse Ion Energization (TIE) region which is an annulus covering all local times but at lower altitudes on the night side. Peterson et al.[14] have noted that the source of the nearly stationary dayside thermal O^+ population with intensity comparable to H^+ at altitudes of 2-3000 km observed just equatorward of the TIE or upwelling ion region is uncertain. These different interpretations are the direct result of a lack of a global view of the cleft ion fountain. Statistical surveys of the fountain from DE-1 produced ion outflow maps where local time and seasonal variations of the outflow were averaged together as the orbit configuration changed. Such averaging makes it impossible to compare ion outflow rates as a function of local time or altitude to determine the extent of the base of the fountain. The ILENA instrument will provide the global view of the base of the cleft ion fountain and TIE regions needed to determine the correct interpretation of previous in situ data (see simulation on the front cover). Using a combination of the PIMS and ILENA measurements, we can thus determine if the source of the stationary O^+ equatorward of the upwelling ion region is photoionization of neutral O at 2,000 km altitudes, simple transport of O^+ from the ionosphere below, or the result of processes driven by the entry of solar wind plasma into the cusp/cleft ionosphere.

2.3. Line-of-sight integration

Using the MSFC model for upwelling ion flux (courtesy Dennis Gallagher) we have performed line-of-sight integration to find the resulting neutral oxygen fluxes (j_O) at the spacecraft location, given by the integral (assuming the source fills the instrument field of view homogenously)

$$j_O = \sigma \int dl j_{O^+} n_H \tag{1}$$

The variation of the $O^+ - H$ cross section with energy is shown in Figure 1, where we plot the data of Fite et al.[25]. The graph show that within the energy range under consideration, i.e., between 30 and 300eV, the cross section varies between 1.05 and $1.35 \times 10^{-15} cm^2$. For a conservative estimate, we take in the following a cross section of $10^{-15} cm^2$. The geocorona neutral hydrogen density is adopted from McComas et al.[26]

$$n_H = 3300 e^{-R/1.6} cm^{-3} \tag{2}$$

Assuming an opening angle of $\Delta\Omega$, and an instrument aperture of A, the neumber of imparting particles per unit time is then given by

$$\frac{\partial N}{\partial t} = A \Delta\Omega j_O = A \Delta\Omega \sigma \int dl j_{O^+} n_H \tag{3}$$

The aperture A, the opening solid angle $\sigma \int dl j_{O^+} n_H$, and the sampling time of the instrument need to be adjusted such that sufficient counts per image will be obtained.

The crucial quantity for this purpose is the neutral oxygen flux j_O at the instrument location. To investigate and predict the flux levels at the spacecraft location, we have performed line of sight integrations of (1). The results are shown in the following section. The center of each image corresponds to a look direction toward a point located at a radial distance of 2 R_E in the noon meridional plane, at an azimuthal angle of 66° out of the equatorial plane. The images represent deviations from this direction, by ±45° in each east or west (horizontal in the image) and north or south (vertical in the image) directions, corresponding to a 90° × 90° field of view. Therefore, the images represent the view and observer would see (if the fluxes were visible), and allow assessment of both the range of flux values dependent of sensor orientation and the angular resolution mandated by source properties.

3. IMAGES AND FLUX AT SPCAECRAFT LOCATION

The cusp/cleft ion fountain model used the source j_{O^+} for the calculations is displayed in a noon meridional cut in the top left panel of color plate 1. The panel represents a 2×2 R_E cut through the center of the Earth. Clearly visible are the cleft ion fountain in the upper right. The enhancement in the lower left is due to the return flux of the oxygen in the model, and will be ignored in the following. The other panels represents the fluxes expected at five locations along the orbit of the HI-LITE Small Explorer (Smith et al., this issue). The locations are (in SM coordinates): $x = -1.29$, $y = -0.72$, $z = 0.09$ (top right panel); $x = -0.74$, $y = -0.81$, $z = 1.42$ (center left panel); $x = -0.05$, $y = -0.75$, $z = 1.65$ (center right panel); $x = 0.26$, $y = -0.72$, $z = 1.60$ (bottom left panel); and $x = 0.99$, $y = -0.63$, $z = 1.08$ (bottom right panel).

The images of plate 1 can be used to estimate the necessary angular resolution of the ILENA instrument. By inspection we find that typical angular dimensions are well in excess of 10°, and that scale lengths for the angular variations are even larger in some cases. Therefore, the planned $6° \times 6°$ field of view per pixel will be sufficient to resolve the most important detail. The relatively large typical variation angle guarantees, furthermore, that the assumption the the source be filling the field of view of an individiual pixel is fulfilled sufficiently well. At last the images show that the cleft ion fountain is well contained in a 90° × 90° field of view as envisioned in the ILENA design (Ghielmetti et al., this issue).

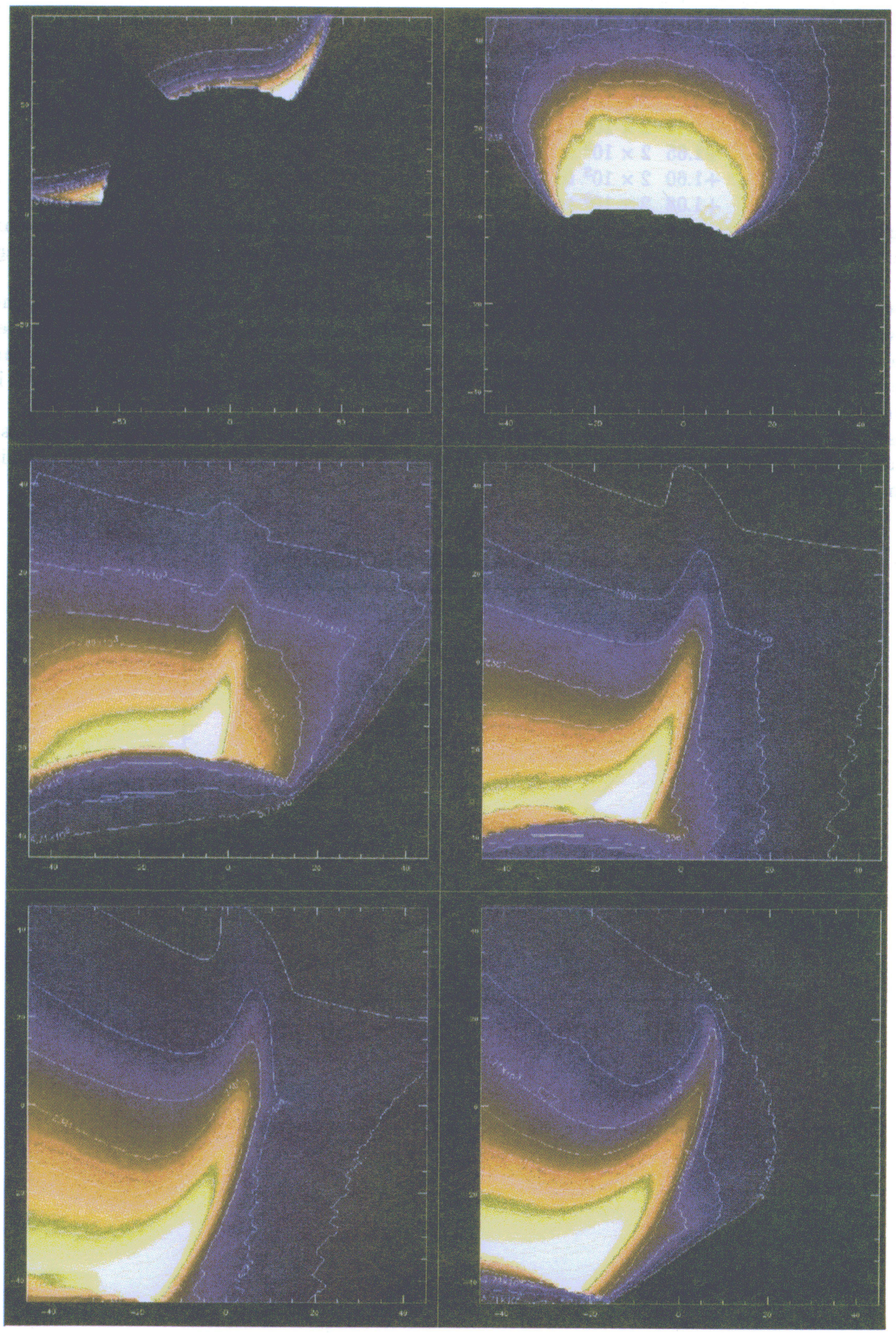

Plate 1: Source and neutral oxygen fluxes in color representation. Each panel corresponds to a $90^o \times 90^o$ field-of-view.

For the purpose of studying the expected range of fluxes, the images of plate 1 are plotted as surfaces and contours in Figures 2-6. These Figures place the emphasis on the maximum and typical ranges of the expeted neutral oxygen fluxes. The results are summarized in the table below

Fig.	x_{SM}	y_{SM}	z_{SM}	Flux Range $/cm^{-2}s^{-1}ster^{-1}$
2	-1.29	-0.72	+0.09	2×10^3 to 4.1×10^3
3	-0.74	-0.81	+1.42	2×10^3 to 1.2×10^4
4	-0.05	-0.75	+1.65	2×10^3 to 8.4×10^3
5	+0.26	-0.72	+1.60	2×10^3 to 1.1×10^4
6	+0.99	-0.63	+1.08	2×10^3 to 9.3×10^3

The Figures show that complete coverage of the ion fountain mandates the capability to image fluxes between about $2 \times 10^3 cm^{-2}s^{-1}ster^{-1}$ and $1.5 \times 10^4 cm^{-2}s^{-1}ster^{-1}$ within a time window determined by magnetospheric processes, of the order of 5min.

As is evident from the plots, typical fluxes are in the range of $2 \times 10^3 - -10^4 cm^{-2}s^{-1}sr^{-1}$ at the spacecraft location, which was chosen to be at a geocentric distance of $2R_E$ in all cases. Therefore we can derive some basic instrument requirements for ILENA: Assuming, say, an angular resolution of $6^o \times 6^o = 9.6 \times 10^{-3} sr$ for each pixel, and an aperture of $1cm^{-2}$ the basic count rate would be $20 - 100s^{-1}$. With an efficiency of 10% taken into account (see Ghilmetti et al., this issue), this reduces to $2 - 10s^{-1}$.

To investigate variations over substorm dynamical time scales, a temporal resolution of about 5 minutes is desirable. In 5 minutes a total of 600−3000 counts would be accumulated. This value is sufficiently high to make an investigation of this kind feasible.

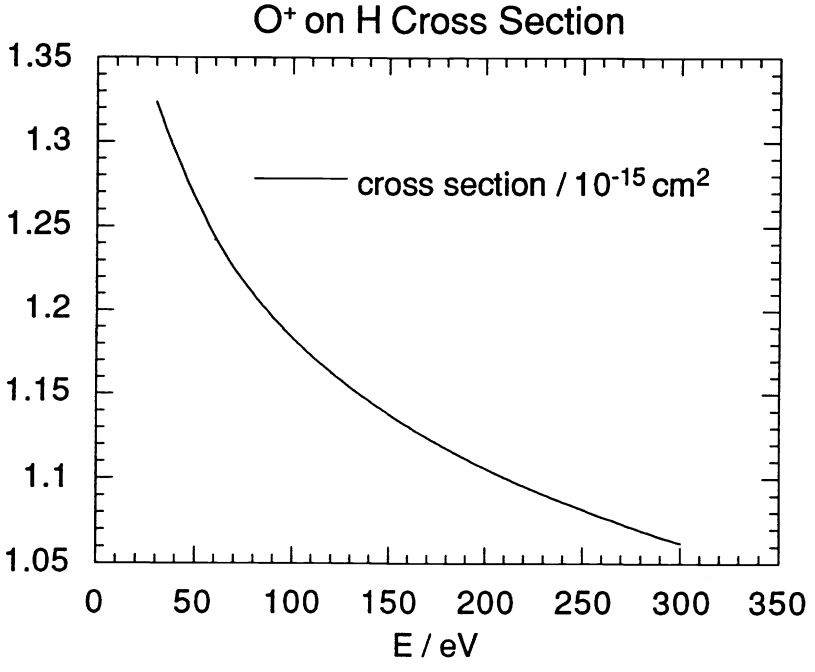

Figure 1. Charge exchange cross section for the reaction $O^+ - H$ vs. energy.

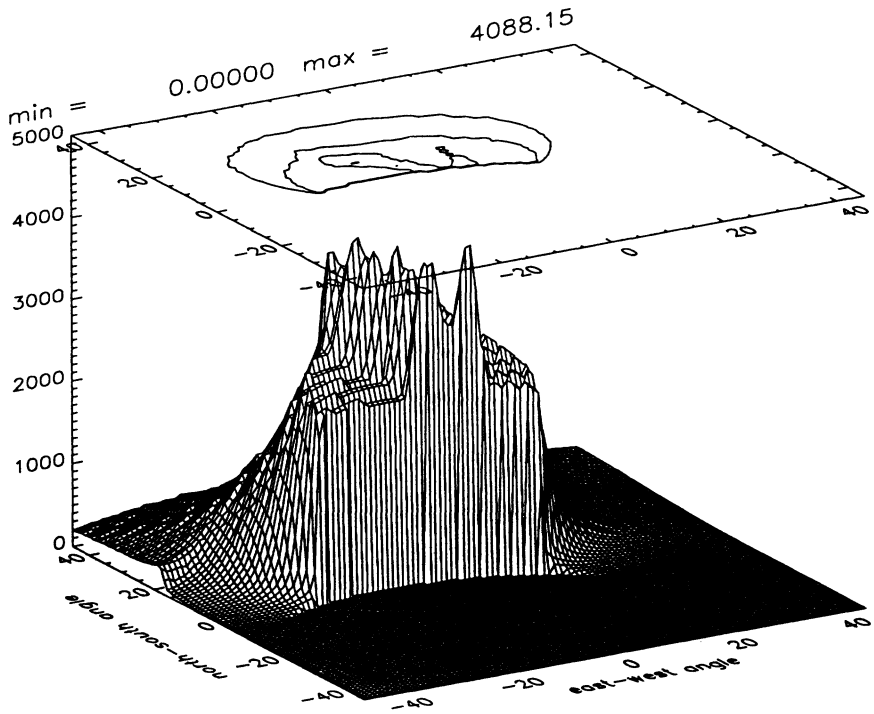

Figure 2. Neutral oxygen flux levels at $x = -1.29$, $y = -0.72$, $z = 0.09$. For comparison, the contours for the angular flux distribution are shown in the top of the figure.

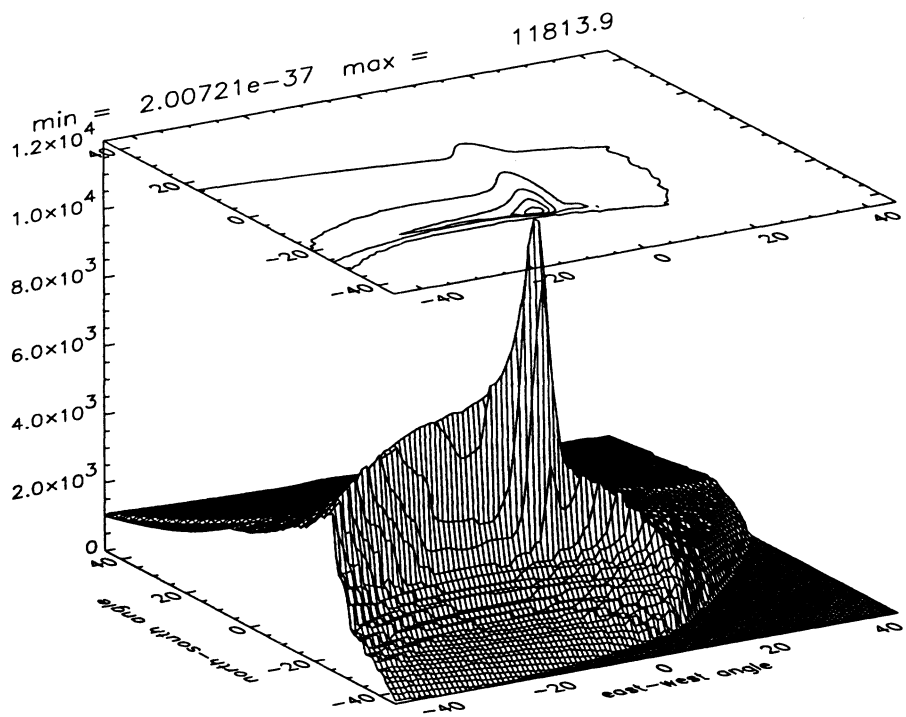

Figure 3. Same as Fig. 2, but at $x = -0.74$, $y = -0.81$, $z = 1.42$.

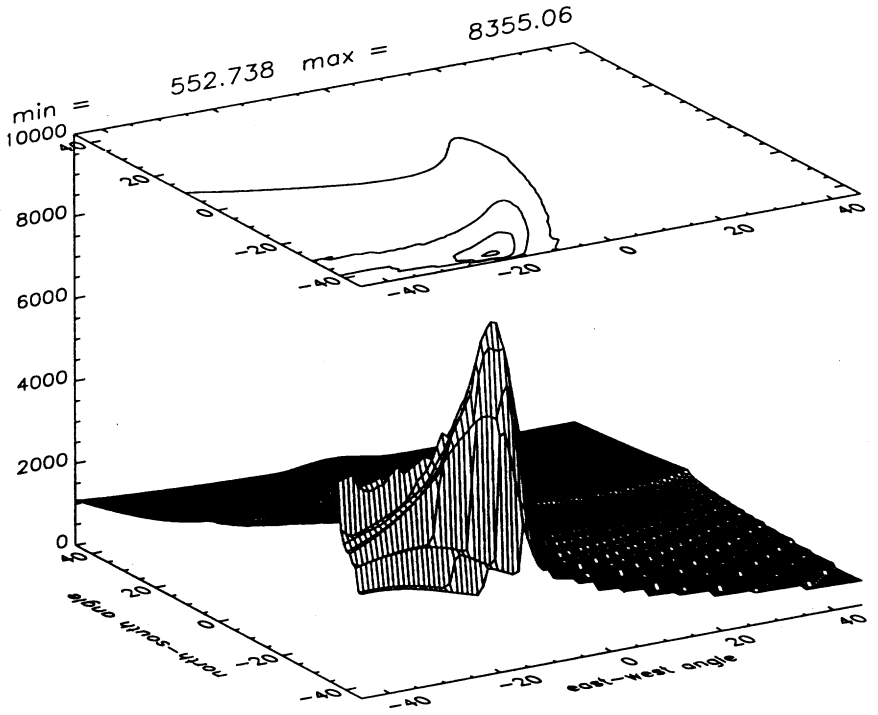

Figure 4. Same as Fig. 2, but at $x = -0.05$, $y = -0.75$, $z = 1.65$.

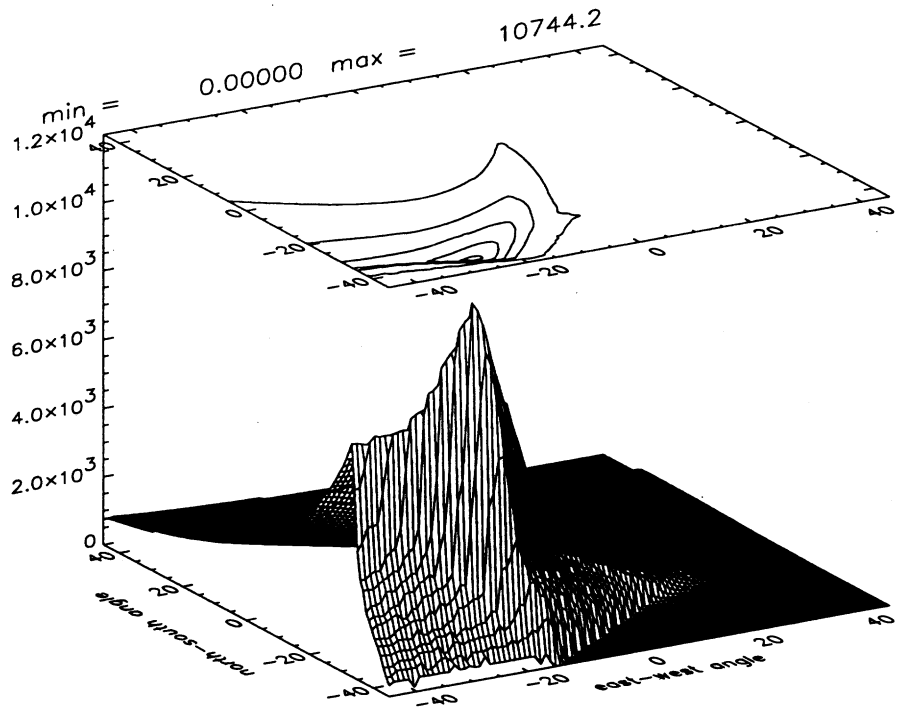

Figure 5. Same as Fig. 2, but at $x = 0.26$, $y = -0.72$, $z = 1.60$.

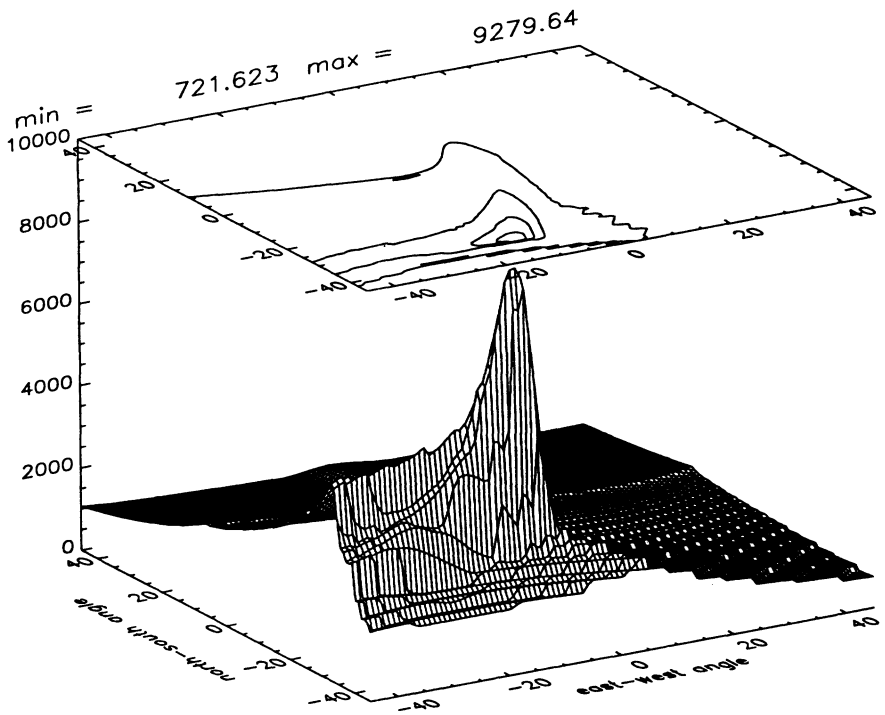

Figure 6. Same as Fig. 2, but at $x = 0.99$, $y = -0.63$, $z = 1.08$.

5. SUMMARY

In this paper we have investigated the expected neutral oxygen fluxes from charge exchange of the cust/cleft ion fountain oxygen ions. The flux distribution in magnitude and look direction was derived for five different orbital locations of the proposed HI-LITE Small Explorer (Smith et al., this issue). The angular distribution of the neutral oxygen flux at the spacecraft location was derived from line-of-sight integration of the source, consisting of the oxygen flux of the cusp/cleft ion fountain, the conservatively estimated charge-exchange cross section, and the geocoronal neutral hydrogen density. Based on the conservatively estimated source, we found flux levels at the spacecraft location to typically fall between $2 \times 10^3 cm^{-2} s^{-1} ster^{-1}$ and about $1 \times 10^4 cm^{-2} s^{-1} ster^{-1}$. Typical angular dimensions, of great importance for instrument design also, appeared to be about 10^o.

These results can be used to derive requirements for instrument design of the ILENA low energy neutral atom imaging instrument (Ghilmetti et al., this issue). Using an instrument efficiency of 10%, an aperture of $1 cm^2$, and a pixel field of view of $6^o \times 6^o$, we found that on a typical substorm dynamical time of 5min between 600 and 3000 counts would be accumulated. This expected number shows that the imaging of the neutral oxygen origination in the cusp/cleft ion fountain region, using the proposed ILENA instrument on the HI-LITE spacecraft is clearly feasible.

6. ACKNOWLEDGEMENTS

This work was supported by NASA.

7. REFERENCES

1. Yau, A. W., E. G. Shelley, W. K. Peterson, and L. Lenchyshyn, Energetic auroral and polar ion outflow at DE 1 altitudes: Magnitude, composition, and magnetic activity dependence and long term variations, J. Geophys. Res., 90, 8417, 1985.

2. Lennartsson W., and E. G. Shelley, Survey of 0.1-16 keV/e plasma sheet ion composition, J. Geophys. Res., 91, 3061, 1986.

3. Chappell, C. R., T. E. Moore, and J. H. Waite, Jr., The ionosphere as a fully adequate source of plasma for the Earth's magnetosphere, J. Geophys. Res., 92, 5896, 1987.

4. Chandler, M. O., J. H. Waite, Jr., and T. E. Moore, Observations of polar ion outflows, J. Geophys. Res. 96, 1421, 1990.

5. Young, D. T., H. Balsiger, and J. Geiss, Correlations of magnetospheric ion composition with geomagnetic and solar activity, J. Geophys. Res., 87, 9077, 1982.

6. Shelley, E. G., Curculation of energetic ions of terrestrial origin in the magnetosphere, Adv Space Res., 5, 401, 1985.

7. Shelley, E. G., Magnetospheric energetic ions from the Earth's ionosphere, Adv. Space Res., 6, 121, 1986.

8. Moore, T. E., C. R. Chappell, M. Lockwood, and J. H. Waite, Jr., Superthermal ion signatures of auroral acceleration processes, J. Geophys. Res. 90, 1611, 1985.

9. Lockwood, M., J. H. Waite, Jr., T. E. Moore, J. F. E. Johnson, and C. R. Chappell, A new source of suprathermal O^+ ions near the dayside polar cap boundary, J. Geophys. Res. 90, 4099, 1985a.

10. Lockwood, M., M. O. Chandler, J. L. Horwitz, J. H. Waite, Jr., T. E. Moore, and C. R. Chappell, The cleft ion fountain, J. Geophys. Res. 90, 9736, 1985b.

11. Waite, J. H., Jr., T. Nagai, J. F. E. Johnson, C. R. Chappell, J. L. Burch, T. L. Killeen, P. B. Hays, G. R. Carrignan, W. K. Peterson, and E. G. Shelley, Escape of suprathermal O^+ ions in the polar cap, J. Geophys. Res. 90, 1619, 1985.

12. Banks, P. M., and T. E. Holzer, High-latitude plasma transport: The polar wind, J. Geophys. Res., 74, 6317, 1969.

13. Moore, T. E., Modulation of terrestrial ion escape flux composition, J. Geophys. Res. 85, 2011, 1980.

14. Peterson, W. K., A. W. Yau, and B. A. Whalen, Simultaneous observations of H^+ and O^+ at two altitudes by the Akebono and Dynamics Explorer-1 satellites, J. Geophys. Res., in press, 1993.

15. Moore, T. E., Superthermal ionospheric outflows, Revs. Geophys. Space Phys. 22, 264, 1984.

16. Shelley, E. G., R. G. Johnson, and R. D. Sharp, Satellite observations of energetic heavy ions during a geomagnetic storm, J. Geophys. Res., 77, 6104, 1972.

17. Baker, D. N., E. W. Hones, Jr., D. T. Young, and J. Birn, The possible role of ionospheric oxygen in the initiation and development of plasma sheet instabilities, Geophys. Res. Lett., 9, 1337, 1982.

18. Lennartsson, O. W., A scenario for solar wind penetration of the Earth's magnetic tail based on ion composition data from the ISEE-1 spacecraft, J. Geophys. Res., 97, 19221, 1992.

19. Daglis, I. A., E. T. Sarris, G. Kremser, and B. Wilken, On the solar wind-magnetosphere-ionosphere coupling: AMPTE/CCE particle data and the AE indices, Proceedings of the 26th ESLAB Symposium - Study of the Solar Terrestrial System, ESA SP-346, p. 193, 1992.

20. McPherron, R. L., C. T. Russell, and M. P. Aubry, Satellite studies of magnetospheric substroms on August 15, 1968, 9, Phenomenological model for substorms, J. Geophys. Res., 78, 3131, 1973.

21. Tsyganenko, N. A., global quantitative models of the geomagnetic field in the cislunar magnetosphere for different disturbance levels, Planet. Space Sci., 35, 1347, 1987.

22. Roelof, E. C., Energetic neutral atom image of a storm-time ring current, Geophys. Res. Lett., 14, 652, 1987.

23. Moore, T. E., M. Lockwood, M. O. Chandler, J. H. Waite, Jr., C. R. Chappell, A. Persoon, and M. Sugiura, Upwelling O^+ ion source characteristics, J. Geophys. Res. 91, 7019, 1986.

24. Whalen, B. A., S. Watanabe, and A. W. Yau, Observations in the transverse ion energization region, Geophys. Res. Lett., 18, 725, 1991.

25. Fite, W. L., A. C. H. Smith, and R. F. Stebbings, Charge transfer in collisions involving symmetric and asymmetric resonances, *Proc. Roy. Soc. London, A268*, 527, 1962

26. McComas, D. J., B. L. Barraclough, R. C. Elphic, H. O. Funsten III, and M. F. Thomsen, Magnetospheric imaging with low-energy neutral atoms, Proc. Natl. Acad. Sci., 88, 9598, 1991.